01 Mar 2023

Enhancement of Heat-Cured Cement Paste with Tannic Acid

Jinrui Zhang

Ziye Kang

Youzhi Yang

Biqin Dong

et. al. For a complete list of authors, see https://scholarsmine.mst.edu/civarc_enveng_facwork/2392

Recommended Citation

J. Zhang et al., "Enhancement of Heat-Cured Cement Paste with Tannic Acid," *Cement and Concrete Composites*, vol. 137, article no. 104931, Elsevier, Mar 2023.
The definitive version is available at https://doi.org/10.1016/j.cemconcomp.2023.104931

Cement and Concrete Composites 137 (2023) 104931

Contents lists available at ScienceDirect

Cement and Concrete Composites

journal homepage: www.elsevier.com/locate/cemconcomp

Enhancement of heat-cured cement paste with tannic acid

Jinrui Zhang [a], Ziye Kang [a], Youzhi Yang [a,*], Biqin Dong [b], Hongyan Ma [c]

[a] State Key Laboratory of Hydraulic Engineering Simulation and Safety, Tianjin University, Tianjin, 300072, China
[b] Guangdong Province Key Laboratory of Durability for Marine Civil Engineering, Shenzhen University, Shenzhen, 518060, China
[c] Department of Civil, Architectural and Environmental Engineering, Missouri University of Science and Technology, Rolla, MO, 65401, USA

ARTICLE INFO

Keywords:
Heat-cured cement paste
Tannic acid
Strength
Microstructure
Molecular dynamics

ABSTRACT

The improvement of cement-based materials' performance by natural organic compounds can greatly promote the green and sustainable development of the construction industry. However, such compounds are not widely used yet because of their retarding effect on cement. In this study, the retardation effect of tannic acid (TA, a well-known retarding compound) is overcome and the enhancing effect is achieved by adding less than 0.1% content and curing samples in thermal regime. Then the mechanism of TA enhancing heat-cured cement pastes is studied systematically. Mechanical properties results suggest that addition of 0.025% TA can reduce the compressive and flexural strengths of cement pastes by up to 3.4% and 17.1% under normal curing regime at 3 days, but enhance these two strengths by more than 11.4% and 34.6% after thermal curing, respectively. XRD patterns and TGA analysis indicate that, under thermal curing regime, 0.025% TA can improve the hydration degree of cement where the bound water content is increased by 21.4%. SEM observations and MIP results show that TA can compact the microstructure and the porosity is decreased by more than 7.0%. Furthermore, FTIR spectrums prove that TA can bond with hydration products. Molecular dynamics simulation demonstrates that TA cross-links with calcium silicate hydrates (C–S–H) through ionic and hydrogen bonds, which could increase the tensile strength by 12.5% and the ultimate strain by 100%.

1. Introduction

Cement is widely used in the construction industry across the world because of good performance and low cost [1,2]. It plays an essential role in many engineering fields, such as construction, transportation, and hydraulic engineering. However, cement is threatening the global environment [3]. The cement industry consumes a lot of energy, with clinker production alone consuming 9.1% of all industrial energy use. It became the second-largest industrial CO_2 emitter, accounting for 27.0% of total industrial carbon dioxide emission in 2020 [4,5]. Besides, the emissions of greenhouse gases and dust can further aggravate photochemical ozone formation, acidification and fresh water eutrophication [6]. This is an unsustainable energy and emission burden for the pursuit of a green world. Thus, there is an urgent need to reduce the amount of cement used.

Enhancing the strength and durability of cement-based materials by adding chemical admixtures or additives is one of the effective approaches to improve the efficiency and reduce the usage of cement [7]. Commonly, the admixtures often used include superplasticizers, antifreeze agents, etc. [8]. The additives could range from nanomaterials (e.g., nano-silica and carbon-based nanomaterials) to fillers and fibers [9,10]. Most of the admixtures are made from polymers, which are oil-based and non-renewable [11]. They can release noxious gas and leach out into environment during the production and use, causing environmental pollution [11]. Besides, commonly used admixtures are generally more expensive than cement. Especially, the cost of nanomaterials is about 1000 times as cement, though the price varies according to type and grade [12]. It would sharply increase the total cost of concrete. Therefore, more environmentally friendly and cheaper materials are needed to improve the properties (e.g., strength) of cement-based materials.

Natural organic extractives from plants can be produced continuously and cheaply [13]. Their successful use to improve the cement-based materials' strength and durability may greatly promote the green and sustainable development of the construction industry. However, the extractives like saccharides, acids and phenols are known as retarders which is deleterious to strength development [14,15]. For example, glucose, mannose and xylose can slow down the cement hydration for up to 2 days [14]. It also has been reported that 0.05% maltodextrin can extend setting time and reduce the 16-h compressive

* Corresponding author.
E-mail address: yangyouzhi@tju.edu.cn (Y. Yang).

https://doi.org/10.1016/j.cemconcomp.2023.104931
Received 15 September 2022; Received in revised form 3 January 2023; Accepted 4 January 2023
Available online 5 January 2023

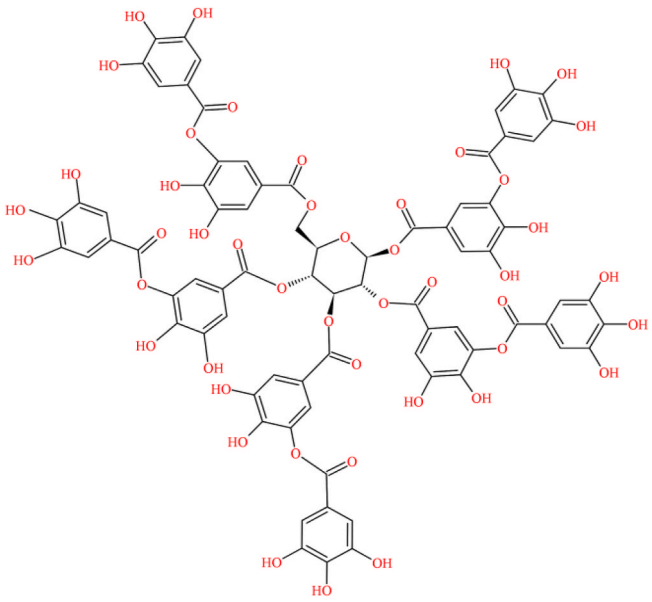

Fig. 1. The molecular structure of TA.

Table 1
The oxide compositions of CPC (%).

CaO	SiO_2	Al_2O_3	Fe_2O_3	MgO	SO_3	K_2O	Na_2O	Others
45.21	25.69	11.42	2.85	5.55	3.44	1.05	0.98	3.81

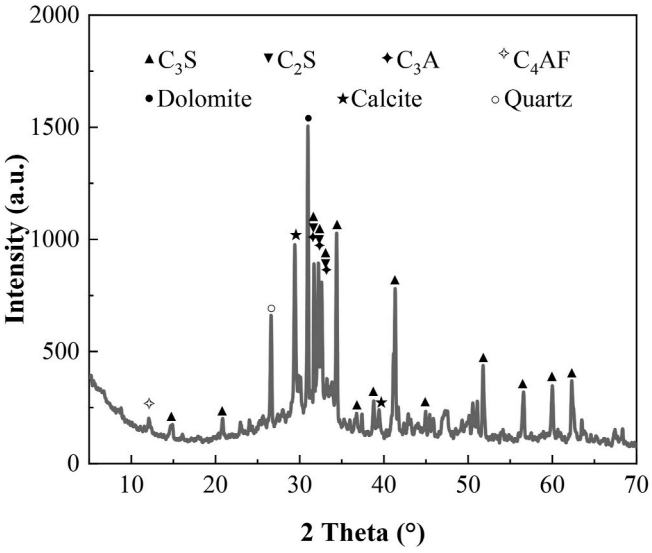

Fig. 2. The XRD patterns of CPC.

strength by 34.1% [16]. Therefore, these extractives have not been widely used in cement yet. But if the retardation is overcome, they could be useful. Zichen Lu et al. [17] eliminated the retarding effect of carboxylated colloidal polymers by adding $Ca(NO_3)_2$ and Na_2SiO_3, realizing almost doubled compressive strength of the blank mortar at age of 12 h. Therefore, we hypothesize that if the retardation problem is solved, the interaction between the natural compounds and cement hydrates can enhance the strength of the cement-based materials.

In this study, tannic acid (TA) is selected to test our hypothesis. As a plant-borne polyphenol, TA widely presents in the leaves, buds and immature fruits of plants [18]. It is green, renewable and cheap, only $1 per kilogram [19]. The molecular formula of TA is $C_{76}H_{52}O_{46}$ and the structure is shown in Fig. 1. It has high catechol content, and therefore possesses capability to strongly bind to diverse surfaces through covalent and non-covalent (e.g., hydrogen bonding) interactions, which makes it a universal linker to functionalize the materials [20,21]. Xinyan Sun et al. [22] used TA to treat magnesium oxychloride cement and found that TA bridges rod-like phase 5 by chelating with Mg^{2+} and improves the water resistance. For portland cement, TA is regarded as a retarder which can enormously increase the setting time and reduce the compressive strength generally by adding more than 0.1% (by weight of cement) [23,24]. However, studies have shown that TA can interact with siloxane sites by virtue of hydrogen bonds and adhere on the surface of concrete firmly [25,26]. These studies show the potential of TA to improve the strength of cement-based materials through cross-linking with hydration products.

In order to suppress the retardation effect and achieve the enhancement of cement pastes by TA, this paper adds less than 0.1% TA by weight of cement and uses heat curing to accelerate hydration. Then the mechanism of TA enhancing cement pastes was studied systematically through comparing the properties under different curing regimes. Mechanical tests were used to quantify the overall effects of TA on cement pastes. X-ray diffraction (XRD) and thermogravimetry analysis (TGA) were arranged to analyze the hydration products evolution. Scanning electron microscopy (SEM) and mercury intrusion porosimetry (MIP) were used to observe the microstructure characteristics. Fourier transform infrared spectroscopy (FTIR) and molecular dynamics simulation were carried out to analyze the interactions of TA with calcium silicate hydrate (C–S–H).

2. Experimental program

2.1. Raw materials and mix proportions

A commercial composite Portland cement (CPC) was used in this study. The oxide compositions of the CPC obtained by X-ray fluorescence are shown in Table 1. The mineral phases tested by XRD are shown in Fig. 2. TA, analytical reagent, was purchased from BKMAM Co., Ltd, China. For the sake of investigating the effect of TA on cement, coarse and fine aggregates were not incorporated into the prepared specimens. All pastes in this research were obtained with a water-to-cement ratio of 0.38. Seven dosages of TA incorporation were set as 0, 0.00625%, 0.0125%, 0.025%, 0.05%, 0.1%, 1% mass ratio of CPC for different tests.

2.2. Mixing, casting, and curing regimes

TA was added into water firstly and stirred until the powder dissolved completely, then mixed with CPC in a mixer for a homogeneous mixing. The obtained pastes were poured into molds with sizes of 50 mm × 50 mm × 50 mm and 40 mm × 40 mm × 160 mm for compressive and flexural strength tests, respectively. The samples were covered with plastic wrap and demolded after one day. To verify the effect of thermal curing, they were compared in different regimes: (1) normal water (NW) curing – the specimens were soaked in 20 °C water until 3, 7, 28 days; (2) hot water (HW) curing – the samples were immersed in 90 °C water and maintained for two days, followed by cooling down naturally and curing in NW until being tested. The relevant curing regime and TA content were used to label the samples. For instance, NW0.025 means the pastes mixed with 0.025% TA and cured under NW regime.

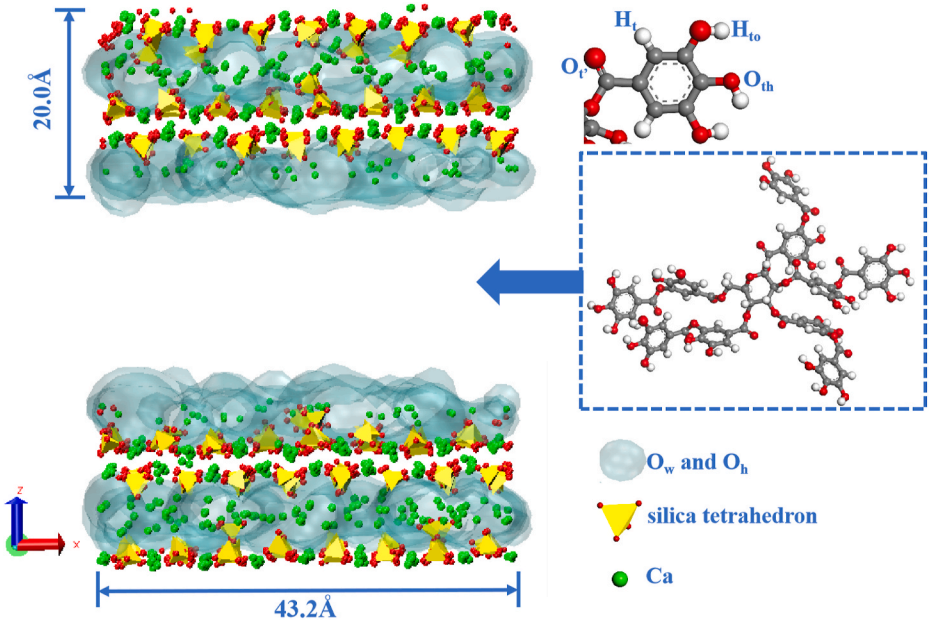

Fig. 3. Schematic diagram of model building.

2.3. Test methods

2.3.1. Compressive and flexural strengths

To explore the effect of TA contents on strength development under different curing regimes, compressive and flexural strengths of cement pastes were tested. Compressive strength was determined using a universal compression test machine with a constant loading rate of 2.4 kN/s. Flexural strength was tested by three-point bending experiment with a loading rate of 50 N/s. The span was set at 100 mm. Six and three specimens were tested at each age to get a reliable result for compressive strength and flexural strength, respectively.

2.3.2. XRD

XRD was performed to observe the changes of hydrates qualitatively. Small slices from the inner part of cube pastes were collected after mechanical tests. They were immersed in isopropanol for 3 days to stop the hydration and further vacuum-dried for at least 3 days. Then all the samples were ground into fine powders passing a 200 mesh sieve. The measurements were conducted using a Rigaku D/MAX-2500PC X-ray diffractometer equipped with a CuKα source. Samples were scanned on a rotating stage between 5 and 70° (2θ) with a step size of 2° (2θ) per minute.

2.3.3. TGA

TGA was used to quantify the hydrates. It was performed with a Mettler Toledo TGA/DSC 2 analyzer. Pastes powders were obtained as described above. Approximately 10 mg of a sample was heated at a constant rate of 10 °C/min from 30 to 1000 °C under a nitrogen flow of 50 mL/min.

2.3.4. SEM

SEM was applied to observe the morphology of the samples (without grinding). Before test, dry samples were vacuumized and coated with gold to increase the conductivity. SEM images were obtained in secondary electron mode with an accelerating voltage of 10 kV.

2.3.5. MIP

MIP was performed to characterize the porous structure of pastes. The particles of samples obtained from the hardened cement pastes were tested. Assuming a cylindrical pore geometry, the applied pressure can be related to equivalent pore sizes using the Washburn equation [27] as given below:

$$P = -\frac{4\gamma\, cos(\theta)}{d} \tag{1}$$

where γ is the surface tension of mercury (0.485 N/m); θ is the contact angle between mercury and the pore surface ($\theta = 130°$); d is the pore diameter (m). MIP parameters were selected based on literature [28]. A volume-weighted pore size distribution can be obtained by associating the intruded mercury volume at a given pressure with the pore size evaluated from Eq. (1) and converted to porosity eventually.

2.3.6. FTIR

FTIR was used to analyze the changes of functional groups to verify the formation of bonds between TA and hydration products indirectly. Analysis was conducted on dried hydrated pastes powder using a PerkinElmer FTIR Spectrometer. The spectrums were traced in the range of 500–4000 cm^{-1}.

2.4. Computational methods

Molecular dynamics simulation can explain the experimental rules from the atomic level and explore the mechanism of modification [29]. In this study, it was used to directly investigate the interaction between TA and hydrates. The main hydration product of cement, C–S–H (with a calcium-to-silicon ratio of 1.7) [30] was selected. The C–S–H structure

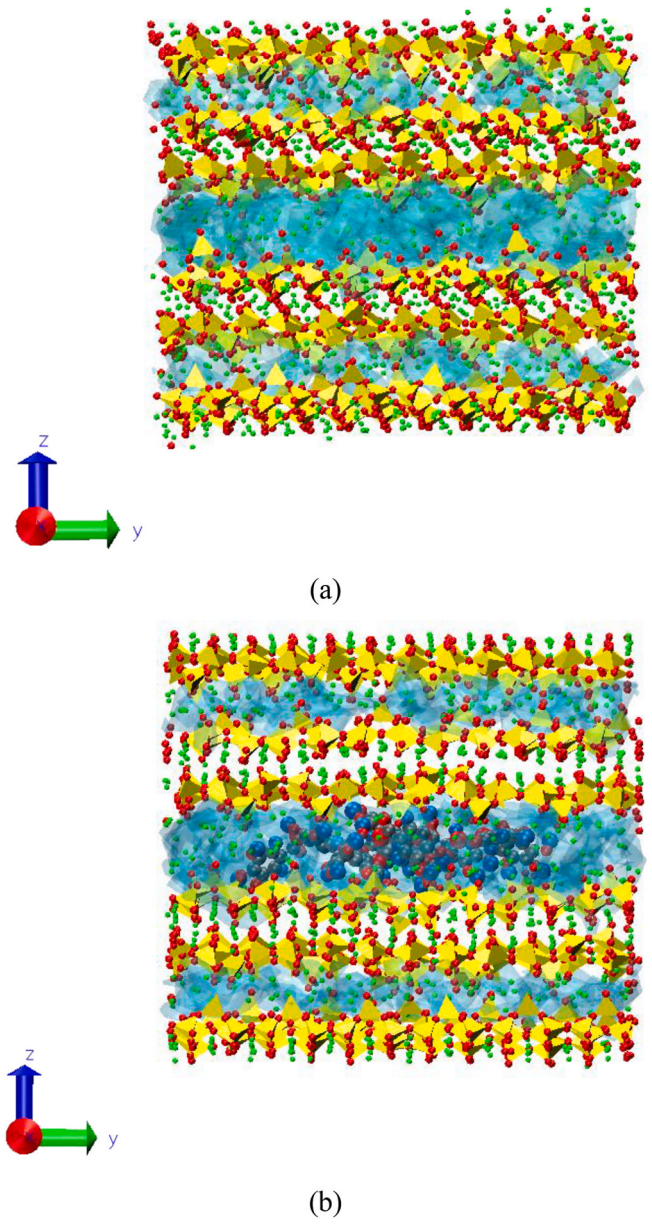

Fig. 4. Equilibrium models of: (a) C–S–H model and (b) TA/C–S–H model.

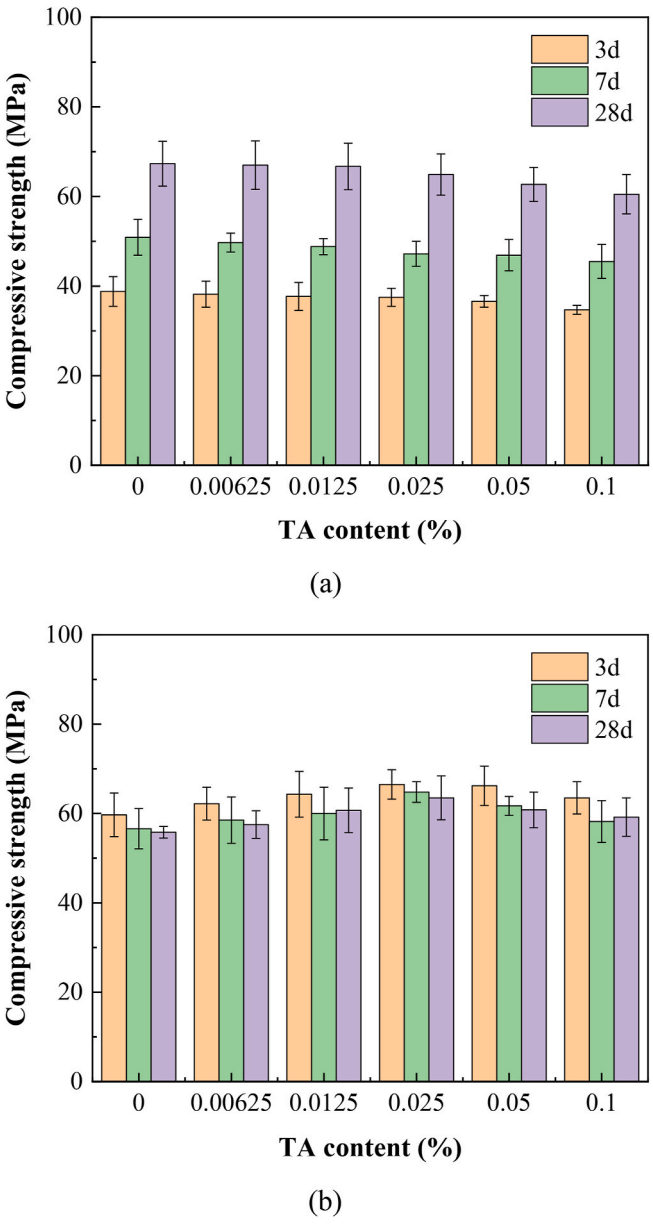

Fig. 5. Compressive strength of cement pastes cured under (a) NW and (b) HW.

was cleaved along with the [0 0 1] crystal plane and TA was inserted in the parallel C–S–H matrix [31]. The constructed TA/C–S–H model is shown in Fig. 3 with unit cell dimensions $a = 43.2$ Å, $b = 45.04$ Å, $c = 92.5$ Å, and $\alpha = \beta = \gamma = 90°$.

The CVFF force field was used to describe the TA and the ClayFF force field was used to simulate the C–S–H phase [32–34]. Geometric rules were used to combine the interaction energy of the two force fields, which can well characterize the properties of nanocomposites [35]. Simulations were performed using LAMMPS software. First, 1 ns relaxation simulations were performed at 300 K and 1 bar in NPT conditions. Then, 1 ns simulations were performed in the NVT conditions. The C–S–H and TA/C–S–H models after dynamic equilibrium are shown in Fig. 4. After equilibrium, 2 ns simulations were continued and the trajectory information was recorded. The models were subjected to uniaxial tensile strain by gradual elongation at a strain rate of 0.00008/ps along the z-direction. The stresses in the x- and y-directions during tension are set to zero and can be relaxed unrestrictedly. The time step of the whole simulation is 1 fs.

3. Results and discussion

3.1. Mechanical properties

3.1.1. Compressive strength

Fig. 5 exhibits the compressive strength of cement pastes with various TA contents and cured in different regimes. As can be seen from

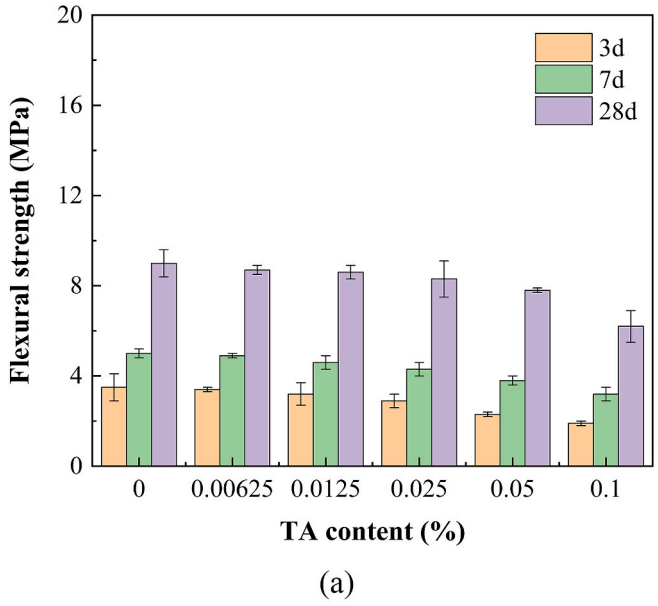

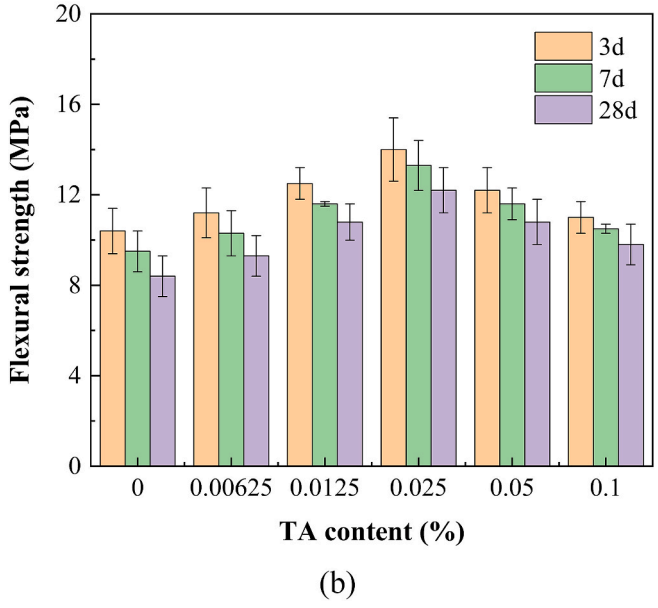

Fig. 6. Flexural strength of cement pastes cured under (a) NW and (b) HW.

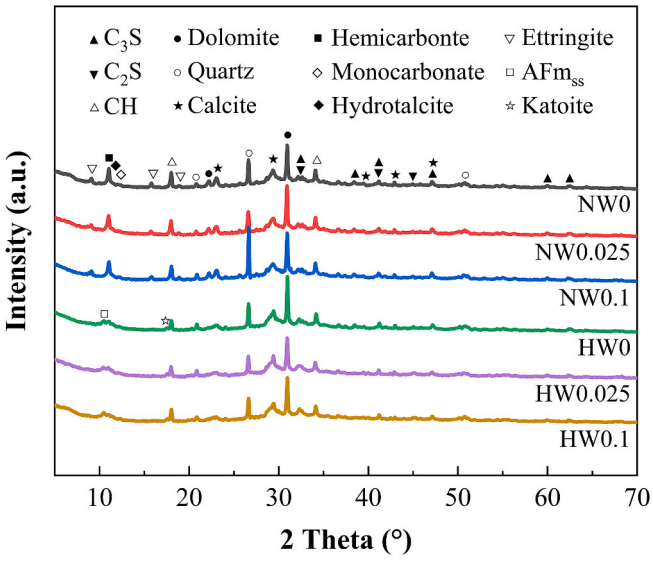

Fig. 7. XRD-patterns of cement pastes cured under NW and HW.

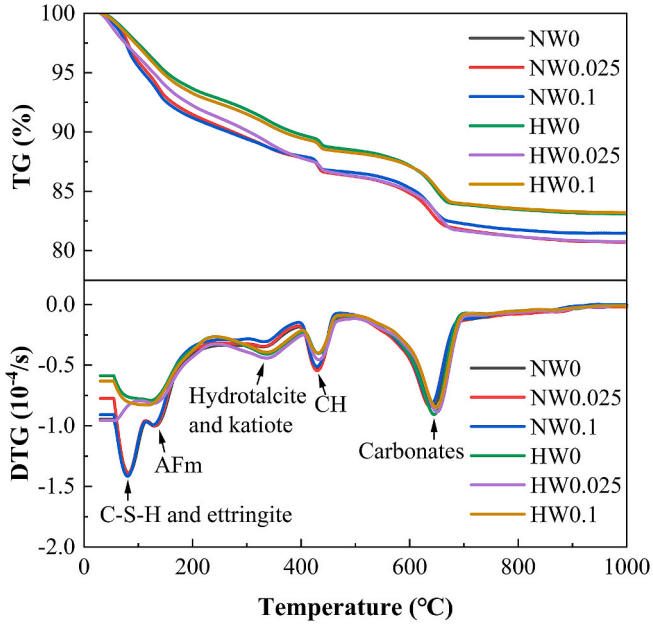

Fig. 8. TGA results of cement pastes cured under NW and HW.

Fig. 5 (a), the compressive strength of NW0 reached 38.8 MPa, 50.9 MPa and 67.3 MPa at 3, 7 and 28 days, respectively. Compared with plain cement pastes without TA, the compressive strength decreased as TA content increases at every age. When 0.025% and 0.1% TA was added, the compressive strength of cement pastes decreased by 3.4% and 10.6% at 3 days, respectively. The tendency of decline remained to the age of 28 days with the extent of 3.6% and 10.1%, which means that less than 0.1% TA also has a profound negative effect on the compressive strength of cement pastes attributed to the retarding (likely nonrecoverable within 28 days) effect of TA [36]. The strong retardation is mainly induced by the adsorption of TA on cement particles and the chelation of dissolved calcium ions by TA molecules, resulting in that less ions (e.g. calcium ions and silica tetrahedron) can precipitate to generate hydration products [36]. Then, we seek to use the HW regime to accelerate the hydration and suppress the retardation effect.

After HW curing, the early compressive strength of cement pastes was improved significantly and reached maximum at 3 days. According to Fig. 5 (b), the 3-day compressive strength of HW0 was 59.7 MPa. With the progress of curing, the compressive strength decreased to 55.8 MPa at 28 days. This could be due to the long-term water-soaking curing at 20 °C aggravating the heat damage made by the high-temperature curing in the first days, which accelerates the dissolving out of calcium ions from C–S–H gels and portlandite (CH) in surface pastes. This pheonomenon has also be observed and explained in Ref. [37]. After

Table 2
The CH and BW contents of samples cured under different regimes.

Samples	NW0	NW0.025	NW0.1	HW0	HW0.025	HW0.1
CH content (%)	7.8	7.6	6.7	6.2	7.4	5.9
BW content (%)	17.1	15.9	15.5	13.1	15.9	13.4

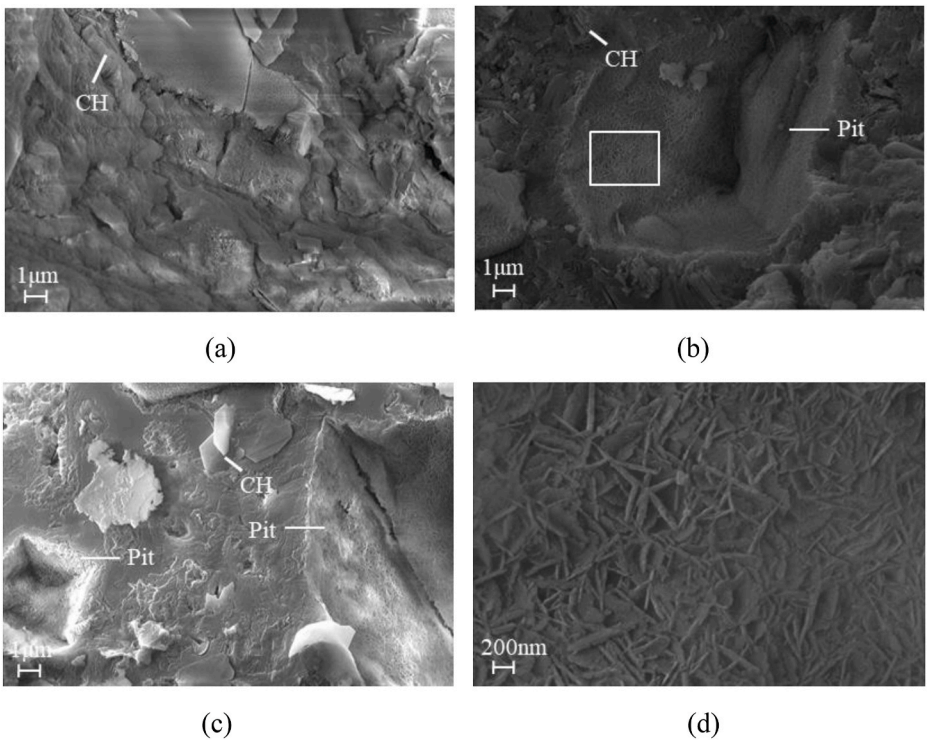

Fig. 9. SEM image of pastes cured under NW. (a) NW0, (b) NW0.025, (c) NW0.1, (d) The enlargement of white box in (b).

adding TA, the compressive strength of the specimen did not show a significant decrease. Compared with HW0, the compressive strength of samples was enhanced by 11.4% (reaching 66.5 MPa) in the best when 0.025% TA was added at 3 days. Meanwhile, the increase was maintained to 28 days with the rate of 13.8%, which demonstrates that the improvement of compressive strength of TA-modified cement pastes is stable. Besides, the compressive strength of HW-cured specimens is always lower than NW0 at 28 days because of the heat damage. During HW curing, the rapid hydration of cement results in coarse hydration products and the expansion of gas-liquid phase produces volume deformation and micro-cracks, which can impair the strength development of concrete [38].

3.1.2. *Flexural strength*

Fig. 6 shows the flexural strength of cement pastes with various TA contents cured in different regimes. From Fig. 6 (a), under NW curing regime, the addition of 0.00625%, 0.0125%, 0.025%, 0.05% and 0.1% TA reduced the 3-day flexural strength of cement pastes by 2.9%, 8.6%, 17.1%, 34.3% and 45.7%, respectively. What is worse, the reduction remained until 7 and 28 days with the extents of 2.0–36.0% and 3.3–31.1%, respectively. The phenomenon was similar with the compressive strength (as shown in Fig. 5 (a)), which may be caused by the retarding effect of TA under normal temperature.

The flexural strength test results of pastes cured under HW are shown in Fig. 6 (b). Consistent with previous studies [39], the flexural strength of plain cement pastes without TA increased significantly after HW curing. Surprisingly, the flexural strength of cement pastes with TA further improved, showing a trend of rising up firstly and then declining. With the increase of TA content from 0.00625% to 0.1%, the flexural strength of HW-cured samples increased by 7.7%, 20.2%, 34.6%, 17.3% and 5.8% at the age of 3 days, respectively. The maximum was reached when the TA content was 0.025%. Although the flexural strength was reduced at 7 and 28 days, that of TA-modified samples was also 8.4–40.0% and 10.7–45.2% higher than HW0, respectively. It should be pointed out that TA seems to be more effective in improving flexural strength than enhancing compressive strength, which is beneficial to deal with the brittleness increase of cement-based materials after thermal curing [40].

According to the mechanical results, TA can enhance the cement pastes under thermal curing. Considering that the 3-day strength of the HW-cured samples is maximum (which is normal according to literature [37]), the mechanism of TA enhancing strength of cement pastes was studied through three representative samples mixed with 0, 0.025% and 0.1% TA at the age of 3 days.

3.2. *Hydration products evolution*

The XRD patterns in Fig. 7 show the hydration products formed in cement pastes mixed with different TA contents at the age of 3 days (cured in two different regimes). Dolomite, quartz and calcite are still the strongest peaks on the patterns. Furthermore, there were no distinguished new diffraction peaks appearing in two regimes, indicating that the presence of TA did not generate new hydration products, which is consistent with previous studies [36]. Under NW curing regime, all samples displayed the presence of ettringite and portlandite. The formation of hemicarbonate instead of monosulfate can be observed too, because the limestone and dolomite in CPC provide CO_3^{2-} favoring the precipitation of carboaluminates rather than monosulfate [41].

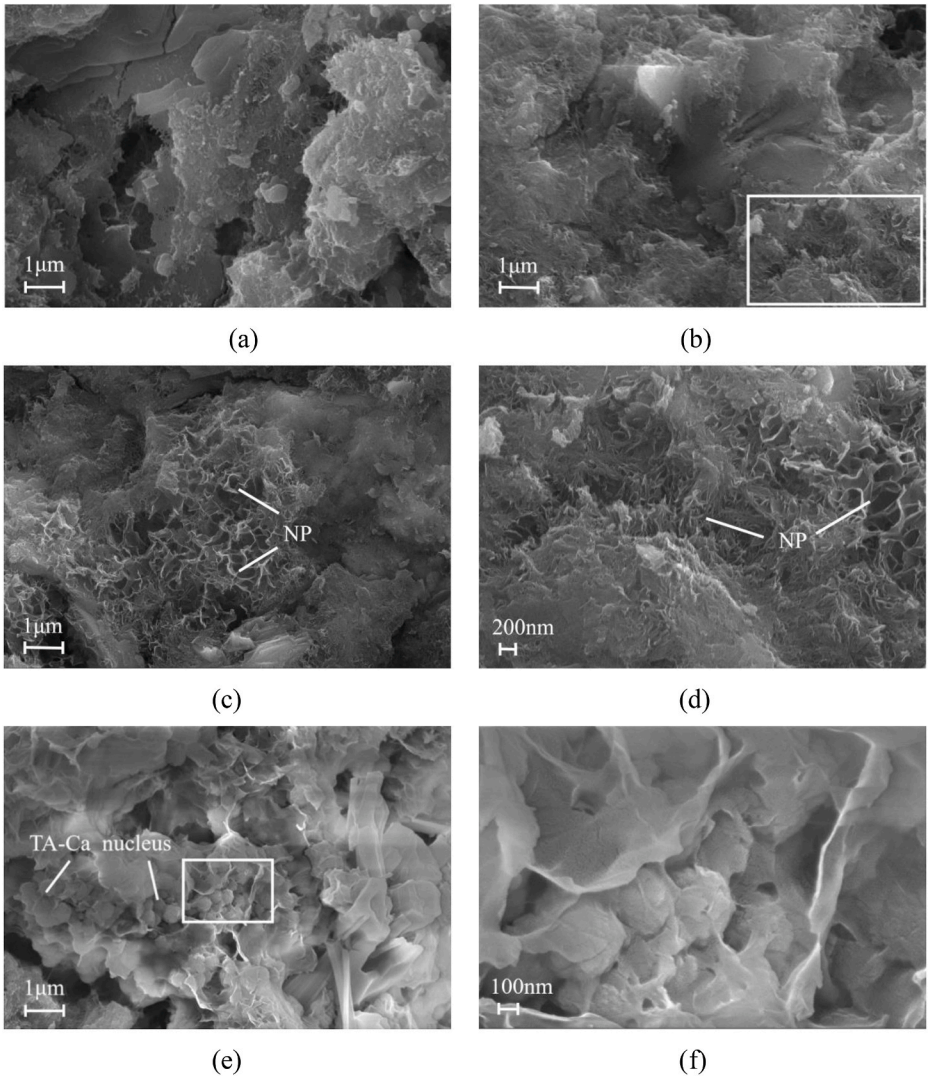

Fig. 10. SEM image of cement pastes cured under HW. (a) HW0, (b) HW0.025, (c) HW0.1, (d) The local increased magnification of image (b), (e) HW1 and (f) The local increased magnification of image (e).

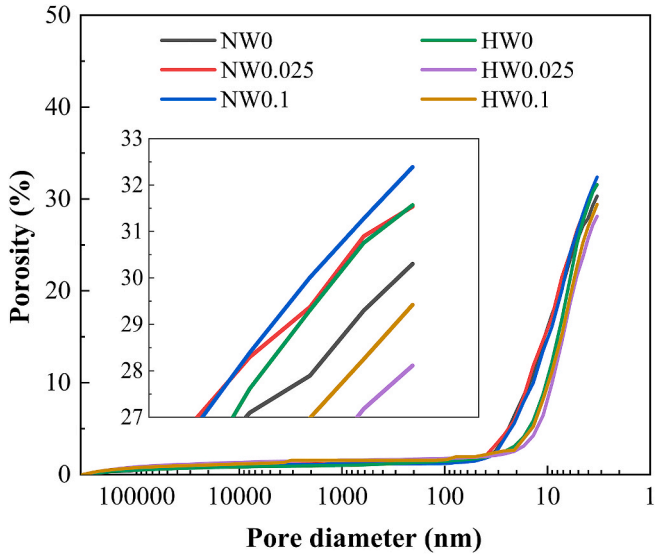

Fig. 11. The porosity of cement pastes cured under NW and HW.

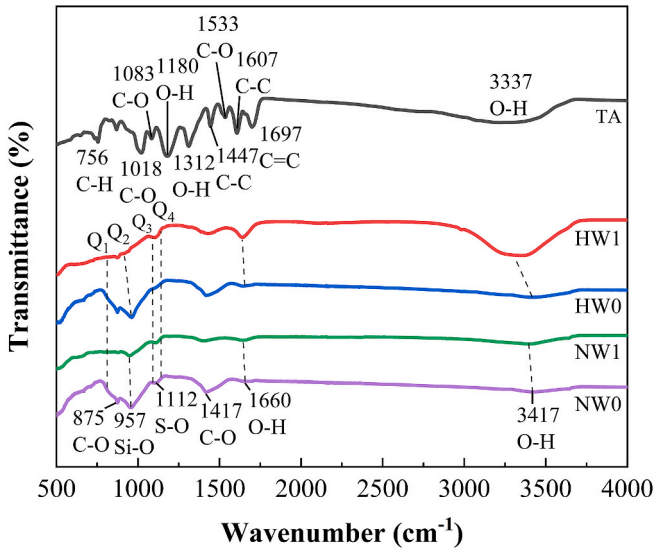

Fig. 12. FTIR spectrums of samples.

Moreover, Mg^{2+} released from dolomite is considered to interact with the cement aluminates to form hydrotalcite [41]. In the case of HW curing, the peaks of ettringite were disappeared and the peaks of hemicarbonate were significantly reduced, which is caused by the decomposition of ettringite and hemicarbonate under high temperature (i.e., during the curing under 90 °C). Meanwhile, katoite and AFm_{ss} which is the solid solution of hemicarbonate and OH^- substituted monosulphate appeared [42]. The effect of TA on these processes is not particularly obvious in XRD patterns. However, by comparing HW0, HW0.025 and HW0.1, it can be found that the peaks of quartz and dolomite decreased significantly after adding TA, qualitatively indicating that TA may promote the hydration of cement under high temperature. To quantitatively verify the effect of TA on cement hydration, TGA test was performed.

TGA tests were carried out on the 3-day specimens. The results are shown in Fig. 8 in terms of the relative mass loss as a function of the temperature (TG, upper y-axis) and the derivative of TG curve (DTG, lower y-axis). On TG and DTG curves, five main peaks were presented, corresponding to C–S–H and ettringite [43], AFm (monosulphate, hemicarbonate and monocarbonate [44]), hydrotalcite and katoite [45,46], CH [47] and carbonates [48], respectively. Before 500 °C, the weight loss of all substances is the bound water (BW). And the mass loss between 400 °C and 500 °C is caused by the decomposition of CH. The contents of BW and CH are often used to assess the degree of hydration and calculated as percentage of the dry pastes weight at 500 °C according to Eqs. (2) and (3) [49]. The results are shown in Table 2.

$$BW = \frac{m_{30} - m_{500}}{m_{500}} \times 100\% \tag{2}$$

$$CH = \frac{m_{400} - m_{500}}{m_{500}} \times \frac{M_{CH}}{M_{H_2O}} = \frac{m_{400} - m_{500}}{m_{500}} \times \frac{74}{18} \times 100\% \tag{3}$$

where m_{30}, m_{400} and m_{500} are the masses of cement pastes at 30 °C, 400 °C and 500 °C, respectively. M_{CH} and M_{H_2O} are the molar mass of $Ca(OH)_2$ and H_2O.

According to the calculated results, CH content of NW-cured samples decreased continuously with the increase of TA dosage. The BW contents of NW0.025 and NW0.1 reduced 7.0% and 9.4% than NW0, respectively. Since all the bound water comes from clinker hydration originally, the reduction of CH and BW contents indicates that TA retards the hydration of cement clinker. However, under HW curing regime, the addition of 0.025% TA increased the CH and BW content by 19.4% and 21.4% than the sample without TA, respectively. It indicates that TA can promote the hydration of the cement clinker under HW curing regime. This may be caused by the polarity of TA which concentrates a large amount of calcium ions and water molecules in its proximity, providing nucleation sites for species dissolved from cement to latch on [50]. Besides, although the CH content of HW0.1 was 4.8% lower than HW0, the BW content of HW0.1 was 2.3% higher than HW0, verifying that TA can promote the secondary hydration of dolomite and quartz under HW curing regime, which is beneficial to strength development of cement pastes. Moreover, the contents of CH and BW of HW0.1 were slightly lower than HW0.025. It may be attributed to the more serious retarding effect of TA in HW0.1, and hence the strength of HW0.1 is lower than HW0.025.

3.3. Microstructure characteristics

Microstructure plays a decisive role in mechanical properties of cement-based materials [51]. In this study, the microstructure of samples cured at 3 days was analyzed including morphology observed by SEM and pore structure tested by MIP.

Fig. 9 shows the microscopic morphology of samples cured under NW regime. From Fig. 9 (a), the sample without TA shows the gelatinous C–S–H and stacked coarse CH. After adding TA, angular pits which are bad for strength development appeared as shown in Fig. 9 (b) and (c). The hydration product in the pit enlarged in Fig. 9 (d) is early C–S–H [52], which will lead to poor bonding of cement particles. Nevertheless, thermal curing changes the condition.

Fig. 10 shows the morphology of samples cured under HW. From

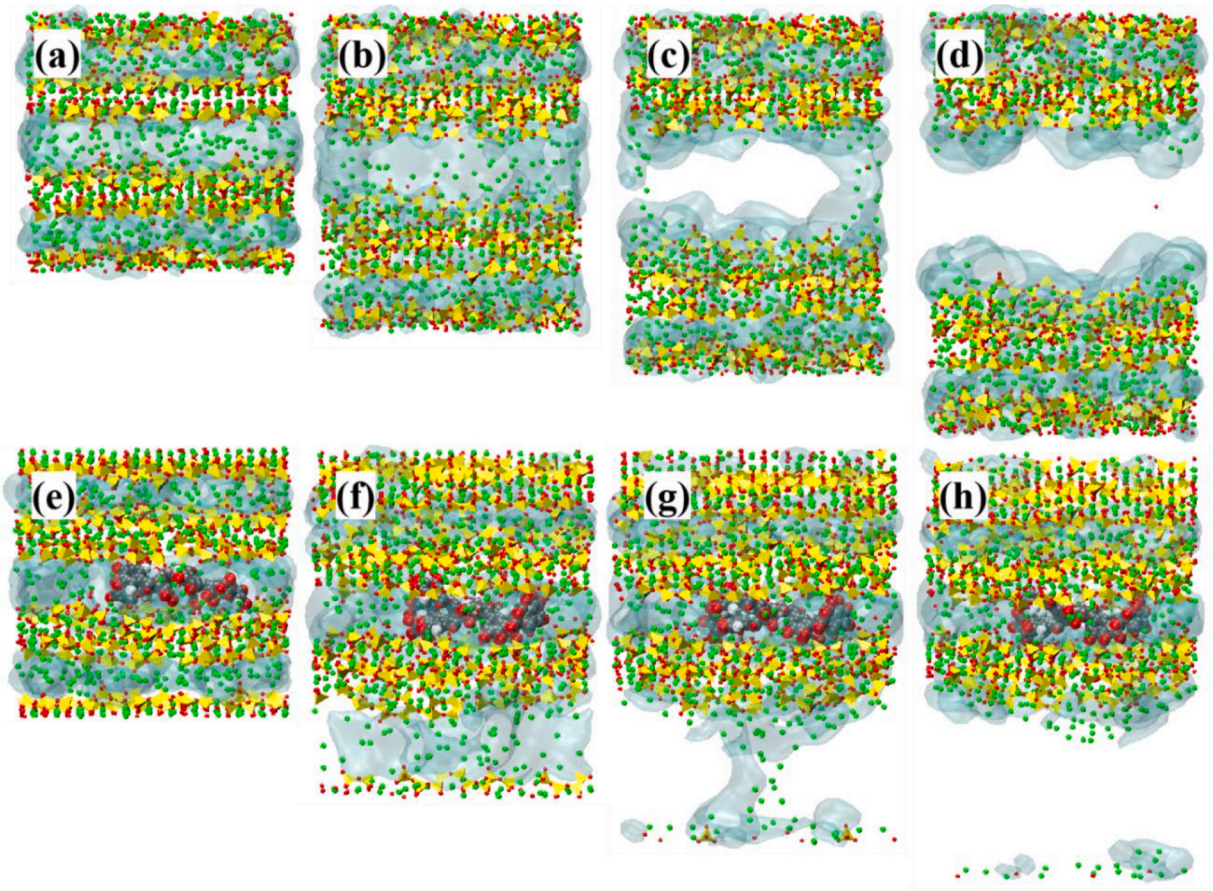

Fig. 13. Diagram of the tensile process under the same strain. (a)–(d) C–S–H model and (e)–(g) TA/C–S–H model at strains of 0.1, 0.4, 0.6 and 0.8.

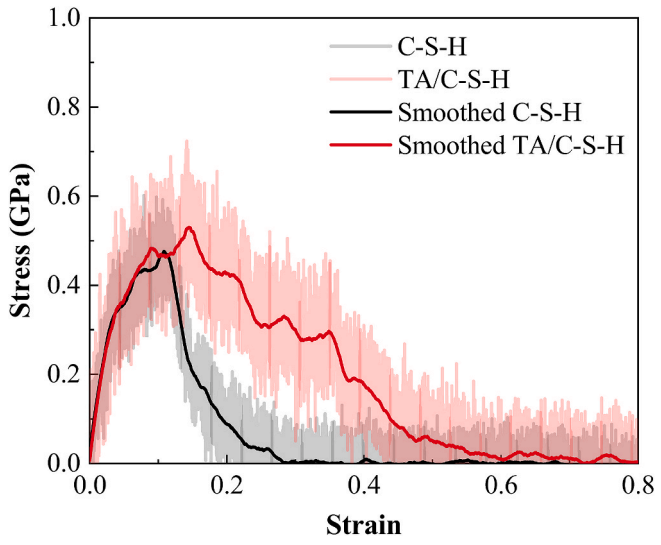

Fig. 14. Stress-strain relations.

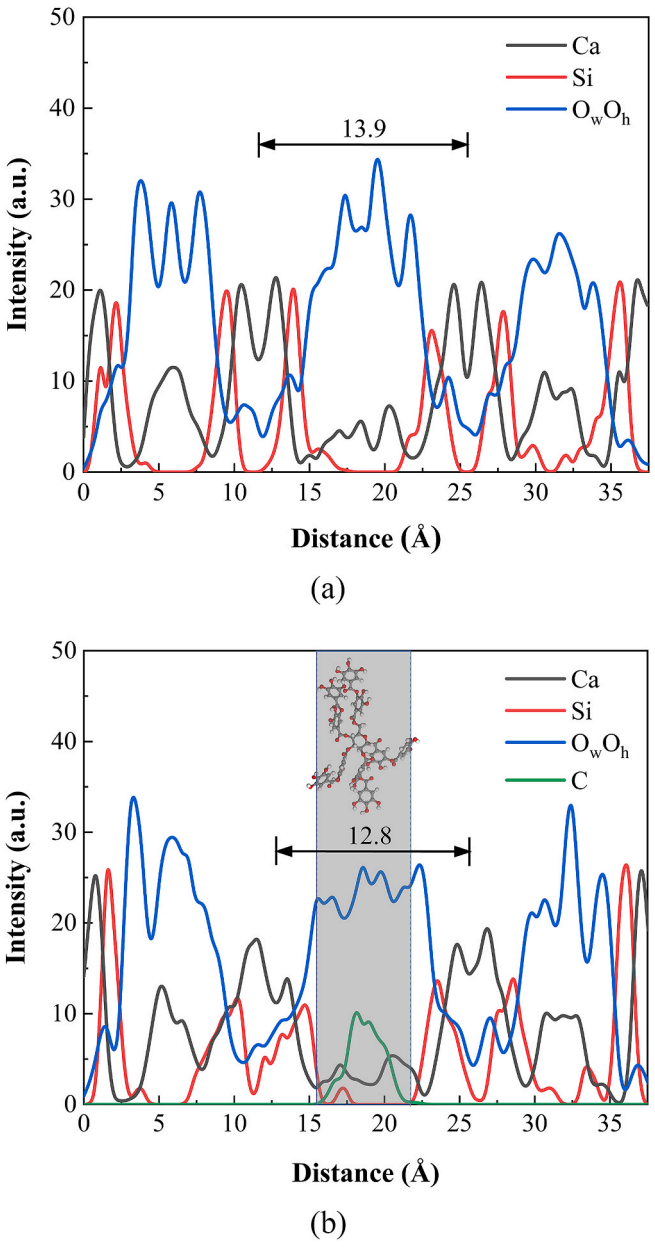

Fig. 15. The intensity profile of the atoms along the interlayer direction. (a) C–S–H model and (b) TA/C–S–H model.

Fig. 10 (a), HW0 exhibited loose and porous structure. After adding TA, the microstructure of HW0.025 became denser as shown in Fig. 10 (b). It is attributed to that TA promotes the hydration of cement which improves the particle packing and TA cross-links with hydration product which makes the particles bond more tightly (given in section 3.4). Besides, nanoscale network hydration products (NP) appeared on the surface of matrix which is enlarged in Fig. 10 (d). Suitable NP can first rupture and consume most of energy when the sample is stretched, thus improving the strength and toughness. However, with the increase of TA content, the NP structure became rougher as shown in Fig. 10 (c). The rough NP structure may be one of the reasons that lead to the strength decrease of HW0.1. Besides, it is difficult to recognize the TA composites which cross-link with hydration products in matrix because of the small dosage.

In order to amplify the influence of TA on microstructure, 1% TA was added. The morphology of HW1 is shown in Fig. 10 (e). Obviously, the NP structure in the matrix became much rougher and a large amount of spherical nanoparticles were detected. The size and shape of nanoparticles are similar to those produced on the surface of TA-modified cement particles and recycled concrete aggregates [53,54]. These nanoparticles are believed to be TA-Ca complexes. In Fig. 10 (f), it is clearly visible that the hydration products generate on the surface of TA-Ca complexes, indicating that the TA composites can cross-link with hydrates and become nucleuses during hydration for the strong adsorption of TA on water and calcium ions [50,55].

Fig. 11 shows the cumulative porosity of pastes mixed with various TA contents. Compared with NW0, the porosity of NW0.025 and NW0.1 increased 4.1% and 6.8%, respectively. On the contrary, addition of 0.025% and 0.1% TA decreased the porosity of cement pastes by 11.1% and 7.0% after accelerating hydration through HW curing. It quantitatively confirms that TA has a positive effect on refining the pore structure of cement pastes under HW curing regime, resulting in a denser microstructure significantly, which is consistent with SEM results as shown in Fig. 10. Moreover, it may be responsible for the increasement of compressive and flexural strength of cement pastes with the addition of 0.025% TA, as shown in Figs. 5 and 6. It is possible that overdosing of TA (e.g., 0.1%) – though possibly results in more hydration products – leads to a network that does not favor load-carrying capacity, and, thus, lower strengths (e.g., than the case of 0.025% TA).

3.4. Interactions analysis

To verify that TA bonded with hydration products observed in Fig. 10 (e), FTIR test was firstly applied on the samples cured at 3 days. The FTIR spectrums are shown in Fig. 12. Under NW curing condition, the peak intensity of Si–O and C–O weakened because of the severe

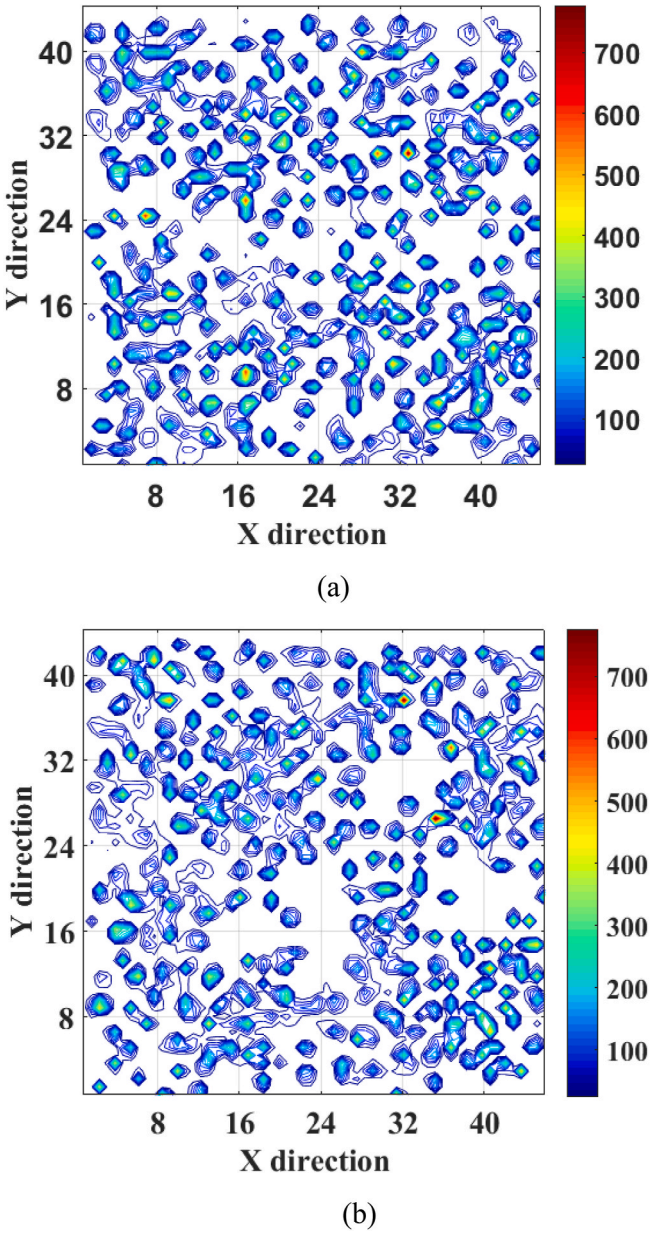

Fig. 16. Contour distribution map of water molecules and hydroxyl groups. (a) C–S–H model and (b) TA/C–S–H model.

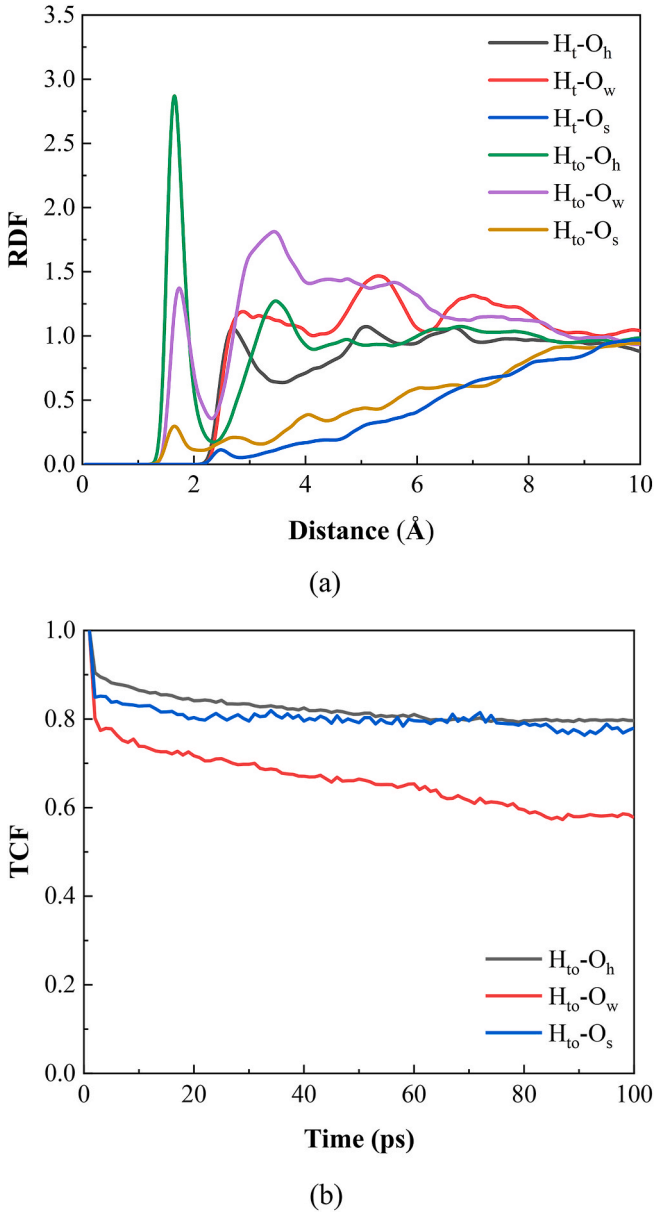

Fig. 17. (a) RDF and (b) TCF of H–O in TA/C–S–H model.

retardation, while the peak position of cement matrix almost unchanged. This indicates that TA has little bond with hydration products under NW. However, the heat-cured samples showed great differences. The peaks centered at 3420 cm^{-1} and 1660 cm^{-1} are the vibration peaks of O–H in the adsorbed water molecules [56]. When TA was incorporated, the peaks of O–H vibration in HW1 strengthened and moved to the left, which proves that TA can absorb on interlayer water through hydrogen bond. Moreover, it has been reported that the hydroxyl group of the polyphenols can interact directly with the siloxane sites by hydrogen bonds [25], which is studied by Q^n in this research. Q represents the tetrahedral unit and *n* is the number of bridging oxygen per tetrahedron [57]. The infrared spectral positions of Q^1-Q^4 are centered at 811 cm^{-1}, 957 cm^{-1}, 1090 cm^{-1} and 1140 cm^{-1} [58]. Results in Fig. 12 indicate that the peaks of Q^1, Q^3 and Q^4 showed little change while the peak of Q^2 changed dramatically. The peak intensity of Q^2 in HW1 weakened after adding 1% TA, indicating that the hydration of cement is delayed severely because of the huge amount of TA. Furthermore, the peak of Q^2 shifted, indicating TA bonds with siloxane sites in C–S–H.

Based on FTIR results, molecular dynamics simulation was arranged to analyze the nanostructure to understand the interaction between TA and hydrates directly. The configurations of the C–S–H model and TA/C–S–H model from strain 0.1 to strain 0.8 are presented in Fig. 13 (a)–(d)

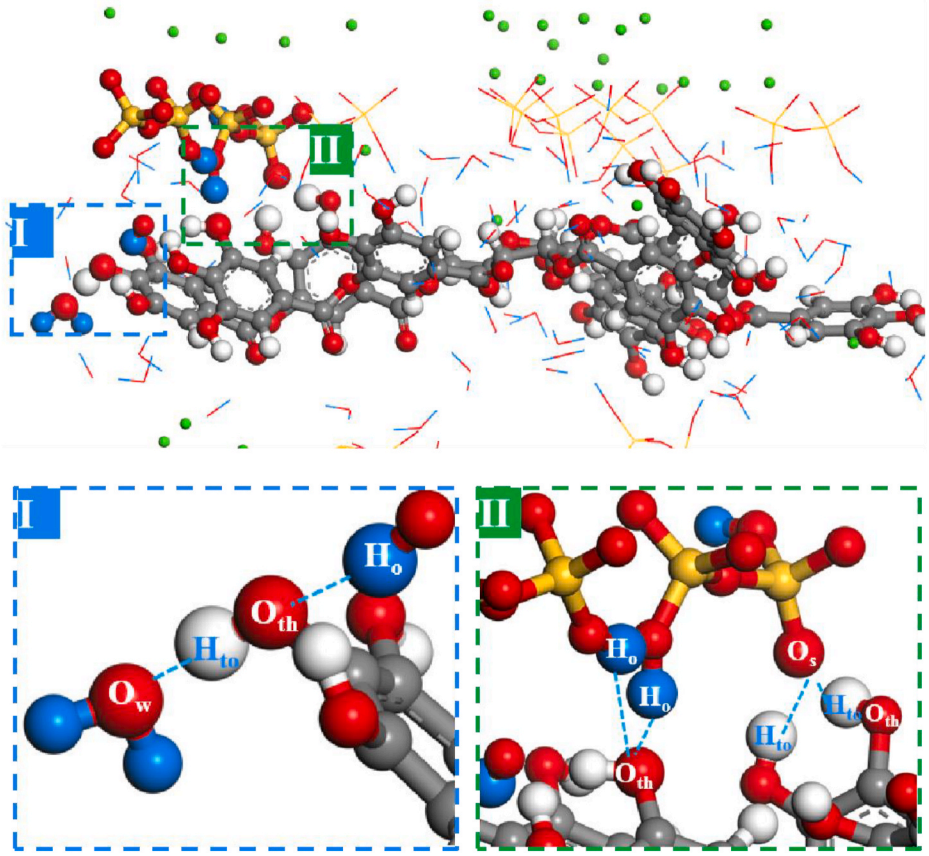

Fig. 18. Local structure of H–O between TA and C–S–H.

and Fig. 13 (e)-(f), respectively, for a preliminary qualitative illustration of the failure process. For the C–S–H model, when the two-layer C–S–H substrate is subjected to tensile loading in the interlayer direction, the model is stretched apart at the interface region of the two-layer matrix. However, in the TA/C–S–H model, the TA effectively bridges the two layers of the matrix and the weak area of the model turns into the interlayer region of the C–S–H structure itself.

The stress-strain relationship of the two models in the tensile process is shown in Fig. 14 and the two are quite different. In the C–S–H model, the stress undergoes a two-stage jump to a maximum value of 0.48 GPa and then decreases rapidly to 0 at the strain of 0.3. After the introduction of TA, the stress jumps to the maximum value of 0.54 GPa in two stages and then slowly decreases after several fluctuations. Finally, it decreases to 0 when the strain is 0.6. Therefore, the tensile strength of the structure after the introduction of TA is increased by 12.5% and the ductility of the structure is greatly improved. The mechanical properties of nano-composites show a better performance of TA in obstructing the propagation of tensile cracks, which could be the reason that the growth of flexural strength of TA-modified cement pastes is higher than that of compressive strength.

Next, two models of the equilibrium state are structurally analyzed to explore the changes brought by the introduction of TA. As shown in Fig. 15, the introduction of TA disturbs the ordered distribution of the calcium-silica layer to some extent and the peak of silica hydroxyl groups at 13.6 Å and 24.2 Å in C–S–H disappeared. Comparing the distance between the calcium layers of the two C–S–H substrates, it can be found that TA decreases the spacing between the two C–S–H substrates (from 13.9 Å to 12.8 Å), which explains the densification of microstructure.

Further statistics on the distribution of water molecules and hydroxyl groups in the range of 15–22.5 Å in the z-direction are shown in Fig. 16. In the C–S–H model, the water molecules and hydroxyl groups in the middle of the two C–S–H matrix layers are distributed in an orderly manner. In contrast, in the TA/C–S–H model, TA occupies the position of water molecules and hydroxyl groups, thus the distribution of water molecules and hydroxyl groups around TA is relatively scattered. This indicates that TA changes the distribution of water molecules and hydroxyl groups around it.

Therefore, the local structures of water molecules and hydroxyl groups in the TA/C–S–H model are also analyzed. H_t (the hydrogen atoms on the carbon chain) and H_{to} (the hydrogen atoms in the phenol hydroxyl group) in TA play a major role and thus their radial distribution function (RDF) with oxygen atoms in C–S–H (O_w, O_h and O_s) are counted, as shown in Fig. 17 (a). The RDF peak confirms that the H_{to} atom forms an H-bond connection with the oxygen atom in C–S–H, while the H_t atom is mostly indirectly connected. Fig. 18 shows the main hydrogen bonding resulting from the introduction of TA; other types of hydrogen bonds are not shown here due to their very small number. The stability of the main H-bonds in the TA/C–S–H system is shown in Fig. 17 (b). The stability of the H-bonds formed between the H_{to} atoms of TA and C–S–H is good, whose time correlation function (TCF) values of the hydrogen bonds remain basically above 0.6 even at 100 ps.

Fig. 19 shows the RDF and TCF statistics of the ionic bonds between the calcium ions of C–S–H and the oxygen atoms of TA. As shown in Fig. 19 (a), both O_{th} and $O_{t'}$ in TA can form ionic bonds with the calcium ions of C–S–H and this structure can be observed in Fig. 20. And Fig. 19 (b) demonstrates that both Ca-O_{th} and Ca-$O_{t'}$ ionic bonds exhibit extreme stability. Especially for Ca-$O_{t'}$, its TCF value remains almost constant at value 1 at 100 ps. Based on the above, it can be seen that TA can achieve the O_1–Ca–O_2 connection with C–S–H, where O_1 can be O_{th} and $O_{t'}$; and O_2 can be O_s, O_h and O_w. Thus, TA realizes the bridging between C–S–H chains.

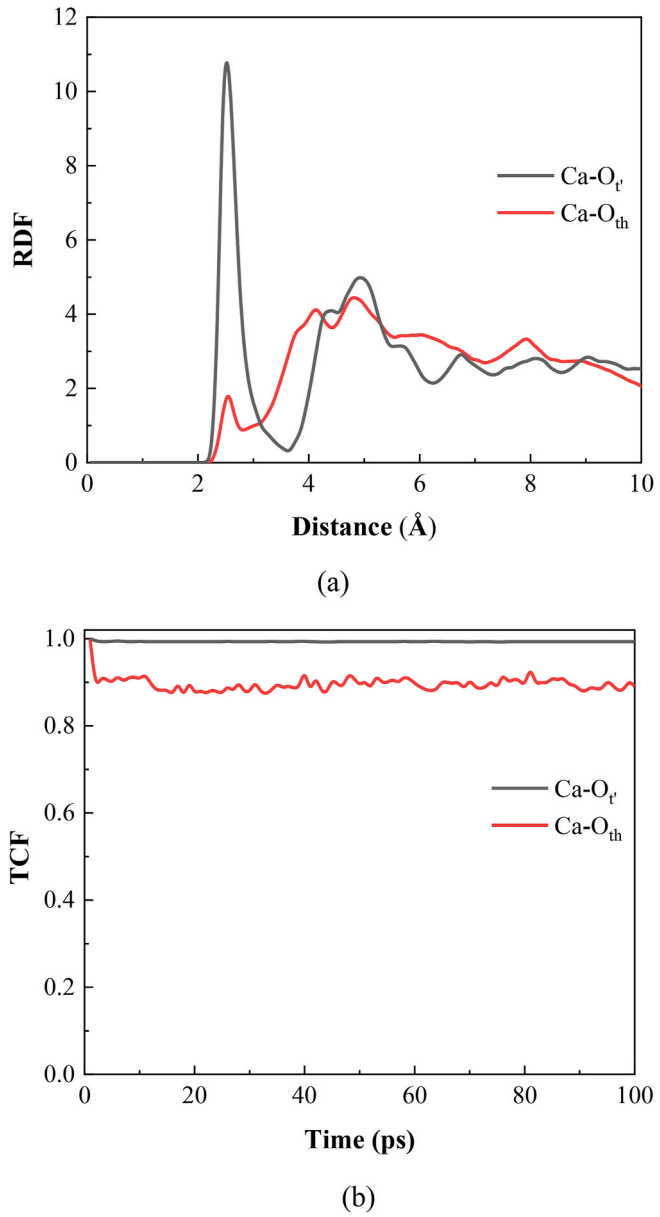

Fig. 19. (a) RDF and (b) TCF of Ca–O in TA/C–S–H model.

Finally, the changes in the dynamic properties of the system atoms are characterized by mean square displacement (MSD). In Fig. 21 (a), by comparing the MSD curves of the main atoms in the TA/C–S–H model, it is clear that the calcium-silica layer of C–S–H has solid kinematic properties and the TA molecules have stronger dynamic properties. Fig. 21 (b) compares the MSD curves of the calcium-silica-oxygen atoms in both systems, where C represents the C–S–H model and T is the TA/C–S–H model. Ca_w is the calcium atoms in the interlayer region of C-S-H. C_t and O_t stand for the carbon and oxygen atoms in TA, respectively. The result reflects that TA accelerates the dynamic properties of the atoms in C–S–H. For example, the MSD value of O_wO_h increases 55.7% from 6.1 $Å^2$ to 9.5 $Å^2$. This also indicates that TA can attract water molecules, hydroxyl groups and calcium ions around them, forming a film-like wrapping structure. When the system is subjected to external loads, this structure helps it to disperse internal stresses and thus achieve greater load resistance. The results in this section are consistent with microstructure results.

The simulation results show that TA can cross-link with C–S–H and improve its dynamic and static mechanical properties at normal temperature. However, in the experiment, the unfavorable interaction between TA and cement particles limited the play of this beneficial effect. Besides, TA molecules were more extended and the contact area with the C–S–H became larger in high temperature, which enhanced interfacial adhesion energy [59]. It also came out that not only the C–S–H had more sites available for TA but also the interfacial ionic bonding formed is more stable after high temperature curing. Therefore, TA exhibited a better ability to enhance the strength of cement pastes at high temperature.

4. Conclusions

In this study, a naturally abundant plant polyphenol – TA, which is often regarded as retarder – was used to modify the cement pastes and the mechanism was systematically studied from mechanical properties, hydration products evolution, microstructure characteristics and interactions analysis. Mechanical results showed that the compressive and flexural strengths of TA-modified cement pastes cured under NW regime decreased with the TA content even if the TA content is less than 0.1%. Microscopic experiments showed that TA can reduce hydration degree and deteriorate the microstructure under normal temperature. These indicate that the enhancement effect of TA cannot be achieved only by reducing the content. Then HW curing was used to speed up the hydration. It is surprising to find that the compressive and flexural strengths can be improved greatly by TA. Optimally, compared with plain cement pastes, the compressive and flexural strengths of 0.025% TA-modified cement pastes can be increased by more than 11.4% and 34.6%, respectively. The mechanism of TA enhancing the cement pastes under HW curing regime should be laid in the followings:

(1) TA can promote the hydration of cement under elevated temperature. XRD and TGA analysis of the hydration products showed that TA can improve the hydration of clinkers as well as the secondary hydration of quartz and dolomite. Quantitatively, the BW content of HW0.025 was 21.4% higher than HW0.
(2) TA can modify the microstructure. More hydration products improve the particle packing in cement pastes and the bridging effect of TA enhances the bonding ability between hydrates, which optimizes the microstructure. SEM observations showed that the matrix became denser after adding 0.025% TA and the TA-Ca complexes cross-linked with the hydration products. In addition, MIP results indicated the porosity can be reduced by more than 7.0%.
(3) TA at proper dosage can bond with hydration products and enhance the tensile strength of nanocomposites. The FTIR spectrums showed the shifts of O–H and Q^2 peak positions which indicated TA can bond with C–S–H indirectly. Besides, molecular dynamics simulation directly proved that TA can cross-link with C–S–H through ionic and hydrogen bonds which can effectively disperse the internal stresses. As a result, the ductility and tensile strength of the composites of TA and C–S–H were enhanced with a 12.5% increased maximum stress and a 100% improved ultimate strain.

Organic compounds are abundant, renewable, safe, and low-cost. They are largely ignored in current concrete research. This paper provides a new insight in the use of organic compounds in cement-based materials and develops new protocols suitable for prefabricated components. Their wide adoption in practice may greatly promote the sustainable development of the construction industry.

Declaration of competing interest

The authors declare that they have no known competing financial interests or personal relationships that could have appeared to influence the work reported in this paper.

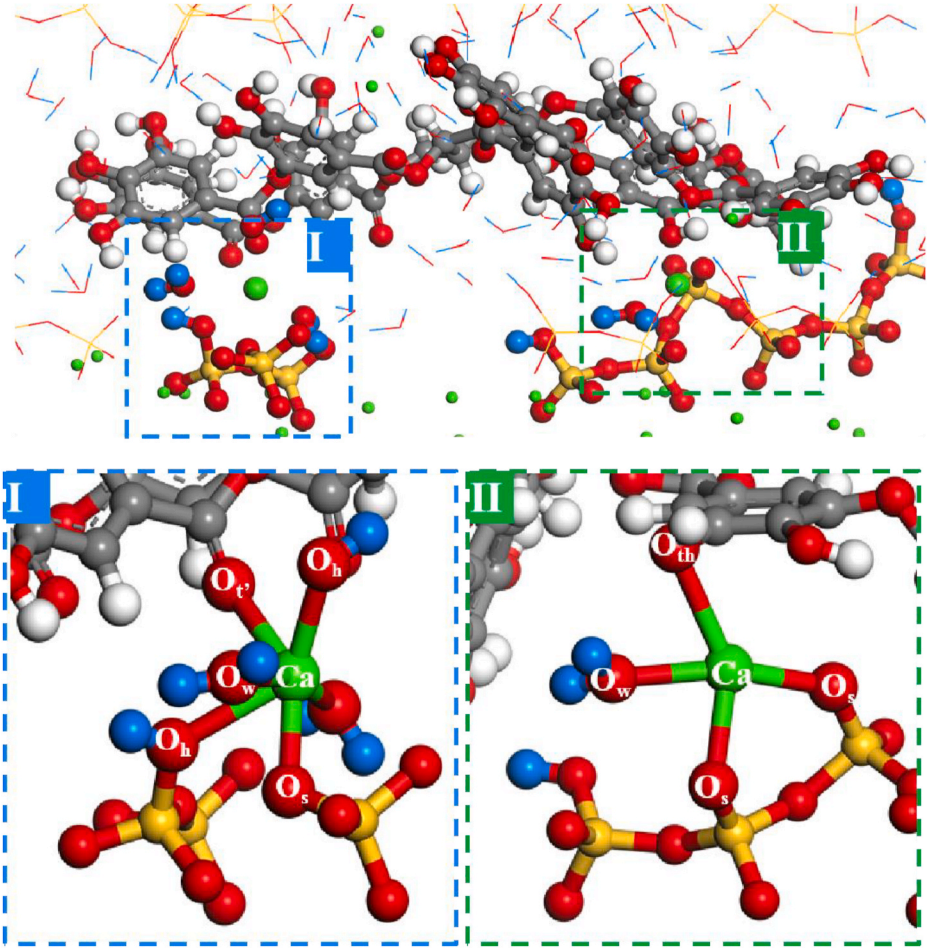

Fig. 20. Local structure of Ca between TA and C–S–H.

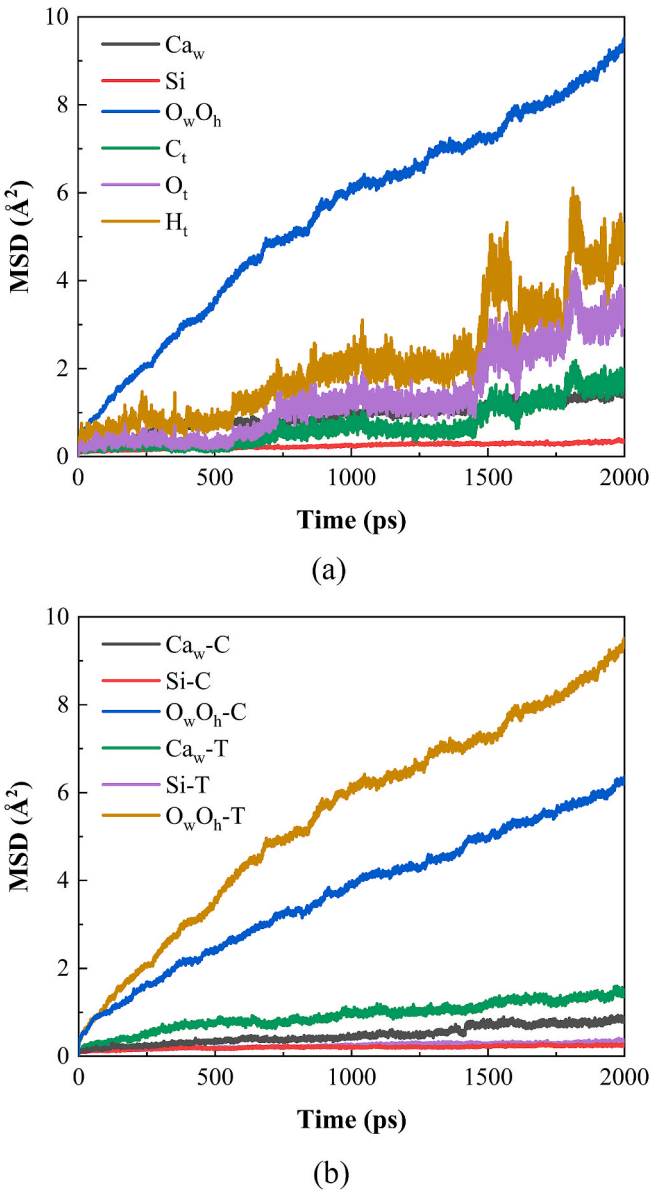

Fig. 21. The MSD for atoms in the (a) TA/C–S–H model and (b) two models.

Data availability

No data was used for the research described in the article.

Acknowledgements

Financial support from the National Natural Science Foundation of China under the grants of 52078332, U2006223 and 51925805 is gratefully acknowledged.

References

[1] Meng Wu, Yunsheng Zhang, Yantao Jia, Wei She, Guojian Liu, Yonggan Yang, Zhidan Rong, Wei Sun, The influence of chemical admixtures on the strength and hydration behavior of lime-based composite cementitious materials, Cement Concr. Compos. 103 (2019) 353–364.
[2] Zongjin Li, Xiangming Zhou, Hongyan Ma, Dongshuai Hou, Advanced Concrete Technology, second ed., Wiley, Hoboken, 2022.
[3] Nabilla Mohamad, Khairunisa Muthusamy, Rahimah Embong, Andri Kusbiantoro, Mohd Hanafi Hashim, Environmental impact of cement production and solutions: a review, Mater. Today Proc. 48 (2021) 741–746.
[4] IEA, Cement, International Energy Agency (IEA), Paris, 2022. https://www.iea.org/reports/cement. (Accessed 9 December 2022).
[5] IEA, Industry, International Energy Agency (IEA), Paris, 2022. https://www.iea.org/reports/industry. (Accessed 9 December 2022).
[6] Diego García Gusano, Israel Herrera, Daniel Garraín, Yolanda Lechón, Helena Cabal, Life cycle assessment of the Spanish cement industry: implementation of environmental-friendly solutions, Clean Technol. Environ. Policy 17 (1) (2014) 59–73.
[7] Karen L. Scrivener, Vanderley M. John, Ellis M. Gartner, Eco-efficient cements: potential economically viable solutions for a low-CO2 cement-based materials industry, Cement Concr. Res. 114 (2018) 2–26.
[8] Alzaza Ahmad, Katja Ohenoja, Isak Langås, Bård Arntsen, Minna Poikelispää, Mirja Illikainen, Low-temperature (−10 °C) curing of Portland cement paste – synergetic effects of chloride-free antifreeze admixture, C–S–H seeds, and room-temperature pre-curing, Cement Concr. Compos. 125 (2022).
[9] M. Ali, Onaizi, Ghasan Fahim Huseien, nor Hasanah Abdul Shukor Lim, Mugahed Amran, and Mostafa Samadi, Effect of nanomaterials inclusion on sustainability of cement-based concretes: a comprehensive review, Construct. Build. Mater. 306 (2021).
[10] Jianwen Shao, Zhu Han, Bo Zhao, Sadi Ibrahim Haruna, Gang Xue, Wenlixia Jiang, Kexiao Wu, Jian Yang, Combined effect of recycled tire rubber and carbon nanotubes on the mechanical properties and microstructure of concrete, Construct. Build. Mater. 322 (2022).
[11] Hersh Faqe, Hoshang Dabaghh, Azad Mohammed, Natural admixture as an alternative for chemical admixture in concrete technology: a review, The Journal of the University of Duhok (2) (2020) 301–308.
[12] Yonathan Reches, Nanoparticles as concrete additives: review and perspectives, Construct. Build. Mater. 175 (2018) 483–495.
[13] T.T. Loan, Vo and Patrick Navard, "Treatments of plant biomass for cementitious building materials – a review, Construct. Build. Mater. 121 (2016) 161–176.
[14] K. Kochova, K. Schollbach, F. Gauvin, H.J.H. Brouwers, Effect of saccharides on the hydration of ordinary Portland cement, Construct. Build. Mater. 150 (2017) 268–275.
[15] V.S. Ramachandran, 2 - research techniques, standards and specifications, Concrete Admixtures Handbook (1996) 69–94.
[16] Lei Lei, Ran Li, Andriana Fuddin, Influence of maltodextrin retarder on the hydration kinetics and mechanical properties of Portland cement, Cement Concr. Compos. 114 (2020).
[17] Zichen Lu, Xiangming Kong, Chaoyang Zhang, Yi Cai, Effect of highly carboxylated colloidal polymers on cement hydration and interactions with calcium ions, Cement Concr. Res. 113 (2018) 140–153.
[18] Kanti Prakash Sharma, Tannin degradation by phytopathogen's tannase: a Plant's defense perspective, Biocatal. Agric. Biotechnol. 21 (2019).
[19] Alice Arbenz, Luc Avérous, Chemical modification of tannins to elaborate aromatic biobased macromolecular architectures, Green Chem. 17 (2015) 2626–2646.
[20] Shuheng Wu, Yujian Yan, Dani Ni, Xianhu Pan Pan, Xin Chen, Jintao Guan, Xuemin Xiong, Liang Liu, Development of a safe and efficient gene delivery system based on a biodegradable tannic acid backbone, Colloids Surf. B Biointerfaces 183 (Nov 1 2019), 110408.
[21] Matthew Korey, Gamini P. Mendis, Jeffrey P. Youngblood, John A. Howarter, Tannic acid: a sustainable crosslinking agent for high glass transition epoxy materials, J. Polym. Sci. Polym. Chem. 56 (13) (2018) 1468–1480.
[22] Xinyan Sun, Qianqian Ye, Wenguang Zhou, Yufei Han, Shanshan Gong, Wenrui Zhou, Sheldon Q. Shi, Jianzhang Li, Zhen Fang, Tannin-modified magnesium oxychloride cement with high-strength and reinforced water-resistance, J. Clean. Prod. 374 (2022).
[23] D.A. Abrams, *Effect of Tannic Acid on the Strength of Concrete* (Structural Research Laboratory), Lewis Institute, Chicago, 1920.
[24] Yi Fang, Jialai Wang, Haibin Ma, Liang Wang, Xin Qian, Pizhong Qiao, Performance enhancement of silica fume blended mortars using bio-functionalized nano-silica, Construct. Build. Mater. 312 (2021).
[25] Kaoru Yamada, Tetsuya Abe, Yoshiaki Tanizawa, Black tea stain formed on the surface of teacups and pots. Part 2 – study of the structure change caused by aging and calcium addition, Food Chem. 103 (1) (2007) 8–14.
[26] Zhong Xiao, Ying Liu, Yuanzhan Wang, Jiafu Shi, TA/Fe(III) anti-chloride coating to protect concrete, J. Clean. Prod. 259 (2020).
[27] Edward W. Washburn, Note on a Method of Determining the Distribution of Pore Sizes in a Porous Material, vol. 7, 1921, pp. 115–116.
[28] Hongyan Ma, Mercury intrusion porosimetry in concrete technology: tips in measurement, pore structure parameter acquisition and application, J. Porous Mater. 21 (2) (2013) 207–215.
[29] Yu Jiao, Heping Zheng, Dongshuai Hou, Jinrui Zhang, Weixiao Xu, Silane coupling agent modification treatment to improve the properties of rubber–cement composites, ACS Sustain. Chem. Eng. 9 (38) (2021) 12899–12911.
[30] Dongshuai Hou, Zeyu Lu, Xiangyu Li, Hongyan Ma, Zongjin Li, Reactive molecular dynamics and experimental study of graphene-cement composites: structure, dynamics and reinforcement mechanisms, Carbon 115 (2017) 188–208.
[31] Yu Jiao, Song Gao, Dongshuai Hou, Pan Wang, Guoxing Sun, Water transport mechanisms of poly(acrylic acid), poly(vinyl alcohol), and poly(ethylene glycol) in C-S-H nanochannels: a molecular dynamics study, J. Phys. Chem. B 124 (28) (Jul 16 2020) 6095–6104.
[32] Randall T. Cygan, Jianjie Liang, Andrey G. Kalinichev, Molecular models of hydroxide, oxyhydroxide, and clay phases and the development of a general force field, J. Phys. Chem. B 108 (2004) 1255–1266.
[33] Oral Büyüköztürk, Markus J. Buehler, Denvid Lau, and Chakrapan Tuakta, "Structural solution using molecular dynamics: Fundamentals and a case study of epoxy-silica interface, Int. J. Solid Struct. 48 (14–15) (2011) 2131–2140.

[34] F. Sanchez, L. Zhang, Interaction energies, structure, and dynamics at functionalized graphitic structure–liquid phase interfaces in an aqueous calcium sulfate solution by molecular dynamics simulation, Carbon 48 (4) (2010) 1210–1223.
[35] Yu Jiao, Dongshuai Hou, JinRui Zhang, Molecular dynamics study on ultra-confined NaCl solution in the silane coupling agent modified rubber calcium silicate hydrate nano-pore, Construct. Build. Mater. 270 (2021).
[36] Yi Fang, Jialai Wang, Xin Qian, Liang Wang, Yijia Dong, Pizhong Qiao, Low-cost, ubiquitous biomolecule as a strength enhancer for cement mortars, Construct. Build. Mater. 311 (2021).
[37] Chao Zou, Guangcheng Long, Cong Ma, Youjun Xie, Effect of subsequent curing on surface permeability and compressive strength of steam-cured concrete, Construct. Build. Mater. 188 (2018) 424–432.
[38] Baoju Liu, Junyi Jiang, Shuai Shen, Feng Zhou, Jinyan Shi, Zhihai He, Effects of curing methods of concrete after steam curing on mechanical strength and permeability, Construct. Build. Mater. 256 (2020).
[39] Yun Duan, Qicai Wang, Zijiang Yang, Xiaoning Cui, Fei Liu, Hai Chen, Research on the effect of steam curing temperature and duration on the strength of manufactured sand concrete and strength estimation model considering thermal damage, Construct. Build. Mater. 315 (2022).
[40] Yu Xiang, Guangcheng Long, Youjun Xie, Keren Zheng, Zhimin He, Kunlin Ma, Xiaohui Zeng, Meng Wang, Thermal damage and its controlling methods of high-speed railway steam-cured concrete: a review, Struct. Concr. 22 (S1) (2020).
[41] Maciej Zajac, Sigrun Kjær Bremseth, Martyn Whitehead, Mohsen Ben Haha, Effect of CaMg(CO3)2 on hydrate assemblages and mechanical properties of hydrated cement pastes at 40°C and 60°C, Cement Concr. Res. 65 (2014) 21–29.
[42] Axel Schöler, Barbara Lothenbach, Winnefeld Frank, Maciej Zajac, Hydration of quaternary Portland cement blends containing blast-furnace slag, siliceous fly ash and limestone powder, Cement Concr. Compos. 55 (2015) 374–382.
[43] Á. Fernández, J.L. García Calvo, M.C. Alonso, Ordinary Portland Cement composition for the optimization of the synergies of supplementary cementitious materials of ternary binders in hydration processes, Cement Concr. Compos. 89 (2018) 238–250.
[44] Maciej Zajac, Anne Rossberg, Gwenn Le Saout, Barbara Lothenbach, Influence of limestone and anhydrite on the hydration of Portland cements, Cement Concr. Compos. 46 (2014) 99–108.
[45] Alisa Machner, Maciej Zajac, Mohsen Ben Haha, Knut O. Kjellsen, Mette R. Geiker, Klaartje De Weerdt, Limitations of the hydrotalcite formation in Portland composite cement pastes containing dolomite and metakaolin, Cement Concr. Res. 105 (2018) 1–17.
[46] Ndigui Billong, U.C. Melo, D. Njopwouo, F. Louvet, J.P. Bonnet, Effect of mixture constituents on properties of slaked lime–metakaolin–sand mortars containing sodium hydroxide, Cement Concr. Compos. 31 (9) (2009) 658–662.
[47] Anjaneya Dixit, Hongjian Du, Juntao Dang, Sze Dai Pang, Quaternary blended limestone-calcined clay cement concrete incorporating fly ash, Cement Concr. Compos. 123 (2021).
[48] Gaifei Peng, Xujing Niu, Yajie Shang, Dengping Zhang, Xiwang Chen, Hong Ding, Combined curing as a novel approach to improve resistance of ultra-high performance concrete to explosive spalling under high temperature and its mechanical properties, Cement Concr. Res. 109 (2018) 147–158.
[49] Binmeng Chen, Hongyu Shao, Bo Li, Zongjin Li, Influence of silane on hydration characteristics and mechanical properties of cement paste, Cement Concr. Compos. 113 (2020).
[50] Changqing Lin, Wei Wei, Yun Hang Hu, Catalytic behavior of graphene oxide for cement hydration process, J. Phys. Chem. Solid. 89 (2016) 128–133.
[51] Qinghua Han, Youzhi Yang, Jinrui Zhang, Yu Jiao, Dongshuai Hou, Biqin Dong, Hongyan Ma, Insights into the interfacial strengthening mechanism of waste rubber/cement paste using polyvinyl alcohol: experimental and molecular dynamics study, Cement Concr. Compos. 114 (2020).
[52] Biljana Ilić, Aleksandra Mitrović, Ljiljana Miličić, Miodrag Zdujić, Compressive strength and microstructure of ordinary cured and autoclaved cement-based composites with mechanically activated kaolins, Construct. Build. Mater. 178 (2018) 92–101.
[53] Liang Wang, Jialai Wang, Xin Qian, Yi Fang, Peiyuan Chen, Atolo Tuinukuafe, Tea stain-inspired treatment for fine recycled concrete aggregates, Construct. Build. Mater. 262 (2020).
[54] Yi Fang, Jialai Wang, Xin Qian, Liang Wang, Peiyuan Chen, Pizhong Qiao, A renewable admixture to enhance the performance of cement mortars through a pre-hydration method, J. Clean. Prod. 332 (2022).
[55] Shuk Ching Tam, J.G. McColl, Aluminum- and calcium-binding affinities of some organic ligands in acidic conditions, J. Environ. Qual. 19 (3) (2009) 514–520.
[56] M.Y.A. Mollah, Wenhong Yu, Robert Schennach, David L. Cocke, A Fourier transform infrared spectroscopic investigation of the early hydration of Portland cement and the influence of sodium lignosulfonate, Cement Concr. Res. 30 (2) (2000) 267–273.
[57] Hans J. Jakobsen Morten Daugaard Andersen, Jørgen Skibsted, Characterization of white Portland cement hydration and the C-S-H structure in the presence of sodium aluminate by 27Al and 29Si MAS NMR spectroscopy, Cement Concr. Res. 34 (5) (2004) 857–868.
[58] I. García Lodeiro, D.E. Macphee, A. Palomo, A. Fernández Jiménez, Effect of alkalis on fresh C–S–H gels. FTIR analysis, Cement Concr. Res. 39 (3) (2009) 147–153.
[59] Yun Zang, Qingrui Yang, Pan Wang, Xinpeng Wang, Dongshuai Hou, Tiejun Zhao, Jianqiang Chen, Molecular dynamics simulation of calcium silicate hydrate/tannic acid interfacial interactions at different temperatures: configuration, structure and dynamic, Construct. Build. Mater. 326 (2022).